Available online at www.sciencedirect.com
SCIENCE DIRECT
International Journal of Mass Spectrometry 245 (2005) 68–77
International Journal of Mass Spectrometry
www.elsevier.com/locate/ijms

Identification of ion fragments produced from thymine and deuterated thymine by low energy ion impact in films and electron impact in the gas phase

Marjorie Imhoff, Zongwu Deng, Michael A. Huels *

Ion Reaction Laboratory, Department of Nuclear Medicine and Radiobiology, Faculty of Medicine, University of Sherbrooke, 3001, 12th Avenue North, Sherbrooke, Que., Canada J1H 5N4

Received 7 May 2005; received in revised form 1 July 2005; accepted 12 July 2005
Available online 18 August 2005

Abstract

The chemical composition of charged fragments desorbing from thymine-methyl-d_3-6-d (T_d) films during 10–200 eV Ar^+ ion irradiation is studied by mass spectrometry of positive and negative ions. The resulting mass spectra are compared to those obtained from similar films of thymine (T), and from 70 eV electron impact on both T and T_d in the gas phase. Ion impact on T and T_d films produces numerous positive and negative ion fragments via endocyclic and exocyclic bond cleavage, even at ion energies well below 60 eV. The major cations desorbing from T films are identified as $HNCH^+$, $HN(CH)CCH_3^+$, $[T–OCN]^+$, $OCNH_2^+$, $C_xH_y^+$ ($x = 1–3$ and $y = 0–4$), and $[T + H]^+$. While ion impact on T and T_d films produces a new fragment $[T–O]^+$, $[T_d–O]^+$, not seen in gas phase electron impact, the latter yields CO^+ fragments that are not observed during ion impact on the films. Anion desorption is dominated by H^-, O^-, CN^-, OCN^-, and $[T–H]^-$ formation, with lesser dissociation channels leading to desorption of C_2^-, C_2H^-, C_2CN^-, $NC_3H_2^-$, $HNC_3H_3^-$, $OC_3H_3^-$, C_2OCN^-, and $C_3H_x^-$ ($x = 2$ and 3). Measurements of the primary ion energy dependence of the fragment desorption yields show that positive ion fragments appear at energies near 15–20 eV, while generally the endocyclic fragments appear at lower energies than the exocyclic (anion and cation) fragments. Our results show that even at very low ion energies, thymine is sensitive to complete fragmentation, whereby the loss of the HNCH (or HNCD from T_d) fragment, i.e., ring cleavage involving the N1 and C6 atoms, dominates; in cellular DNA, this would correspond to complete loss of the base.

Keywords: DNA bases; Ion impact; Ion desorption; Condensed phase

1. Introduction

Ionizing radiation (protons, heavy ions, electron, X- and γ-rays) treatment of biological media causes severe damage to DNA mainly by producing single and double strand breaks of DNA and complex clustered lesions [1]. This damage is associated with abundant secondary particles produced along the radiation tracks, which include low-energy ions, radicals, and ballistic secondary electrons [2,3]. Traditionally, DNA damage has been linked to thermal, or solvated, secondary electrons, and the formation of reactive radicals [4]. Hence, in the past decades, most experimental studies have focused on DNA damage by free radicals and solvated electrons.

However, most of the secondary electrons created along ionizing radiation tracks in solids and liquids have non-thermal initial energy distributions below 100 eV, with a most probable energy below 10 eV. Some secondary electrons such as Auger electrons may have energies up to several 100 eV, or a few kilo electron volts for “delta rays”. Non-thermal secondary electrons can also produce secondary ions, by either ionization, excitation, or dissociative electron attachment (resonances). Recently, this has been shown to cause severe damage to DNA and its components at electron energies as low as 3 eV via resonant mechanism [5–11].

Simultaneously, hyperthermal ($E < 100$ eV) secondary ions are created along any radiation track as a result of dis-

* Corresponding author. Tel.: +1 819 346 1110x14907; fax: +1 819 564 5442.
E-mail address: michael.huels@USherbrooke.ca (M.A. Huels).

1387-3806/$ – see front matter © 2005 Elsevier B.V. All rights reserved.
doi:10.1016/j.ijms.2005.07.002

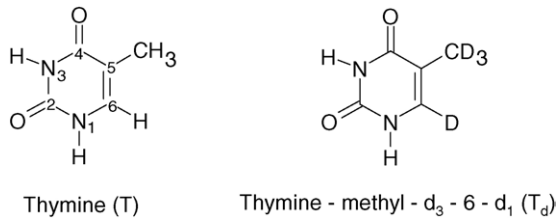

Fig. 1. Molecular structures of thymine (T) and thymine-methyl-d_3-6-d (T_d).

sociative ionizations. High energy electrons or photon tracks usually produce secondary ions with low kinetic energies (typically below 10 eV), but with different chemical reactivities. Some of the ions formed via Auger-decay of specific core excitations can have energies of several tens of electron volts. More important for the present studies, during heavy ion therapy [12,13], secondary atomic ions with energies of several hundred electron volts and multiple charge states can be produced [14]. Furthermore, while heavy ion therapy relies on the ion's highly localized relative dose distribution (Bragg peak), the primary ion's linear energy transfer is highest at the ion track ends where the ionization density is highest, and where the primary ion energy is reduced below a few kilo electron volts. Thus, the chemical and kinetic damage produced by either track-end primary ions, or hyperthermal secondary ions in subsequent scattering events, is of great biological relevance in heavy ion therapy, since it will occur over short distances (a few nanometers) and result in complex DNA damage clusters that cannot be easily repaired by the cell.

In a recent preliminary study [15], we have found that ion impact on condensed phase thymine, at ion energies below 200 eV, results in significant film degradation via both kinetic and potential scattering (i.e., the primary ion's potential energy). However, to understand the sequence of events leading to DNA damage during irradiation requires a detailed knowledge of the initial fragmentation pathways and products, and the possible reactivity of the initial fragments. Thus, the identification of the chemical composition of the fragments produced by ion (or electron) irradiation is a prerequisite for the further study of their reactivity.

Here, we report detailed mass spectroscopy measurements of the energetic (1–5 eV) anion and cation fragments produced by 10–200 eV Ar^+ ion impact on condensed phase thymine-methyl-d_3-6-d (T_d) and thymine (T), with molecular structures shown in Fig. 1. The resulting ion stimulated desorption (ISD) mass spectra are compared to those produced in the same experimental set-up from gas phase T and T_d by 70 eV electron impact, and the chemical identity of fragments produced by ISD is determined.

Our results show that the most abundant cation fragments produced by hyperthermal Ar^+ impact are $HNCH^+$, $HN(CH)CCH_3^+$, $C_3H_3^+$, $OCNH_2^+$, $[T–OCN]^+$, and $[T–O]^+$, where the first two are found to result from specific ring cleavage at, respectively, the C2–N1 and C6–C5, and C2–N1 and C5–C4. For $[T+H]^+$ formation, we find a strong 4:1 preference for abstraction of nitrogen-bound hydrogen from adjacent T, relative to carbon-bound hydrogen, opposed to the stoichiometric NH to CH ratio of 1:2. The most prevalent desorbing anions include H^-, O^-, CN^-, OCN^-, and $[T–H]^-$ formation; the latter involves deprotonation almost exclusively via NH bond cleavage, while H^- formation occurs with stoichiometric ratio from NH and CH sites. Lesser dissociation channels also lead to desorption of OH^-, C_2^-, C_2H^-, C_2CN^-, $NC_3H_2^-$, $HNC_3H_3^-$, $OC_3H_3^-$, C_2OCN^-, and $C_3H_x^-$ ($x=2$ and 3). Here, OH^- (or OD^- from T_d) formation likely involves subsequent reactive scattering of O^- prior to desorption, leading to H abstraction from NH and CH bonds. More importantly, both exocyclic and endocyclic fragmentation is observed for ion beam impact well below 1 eV/amu, and results in the formation of ions that still have sufficient kinetic energy (>1 eV) to overcome the charge induce polarization barrier at the film surface and desorb into the vacuum.

2. Experimental method

The experiments were carried out on an ion beam apparatus developed in-house [15], and which will be discussed in detail elsewhere. Here, we give only a brief description of the experimental method: a low energy ion beam system delivers a highly focused, mass- and energy-resolved positive or negative ion beam in the 1–500 eV energy range into a UHV (10^{-9} Torr) reaction chamber for sample film irradiation. A high resolution quadrupole mass spectrometer (QMS) (Hiden Analytical Ltd.) is installed perpendicularly to the ion beam line to monitor desorbing positive and negative ions *during* ion impact. A large diameter lens is used at the mass spectrometer entrance to ensure a large solid angle of acceptance and thus a higher sensitivity. The QMS is optimized to detect ions of up to 5 eV kinetic energy.

In this work, we focus mainly on 10–200 eV Ar^+ ion irradiation of 200 ng/cm^2 thymine (T and T_d) films on Pt substrates, corresponding roughly to four *nominal* monolayers of thymine assuming no clustering of the molecules [8]. For negative ion desorption, we use 20 ng/cm^2 films. Films are prepared by in vacuo evaporation onto an atomically clean polycrystalline Pt substrate held on a manipulator at room temperature (22–24 °C), while the thymine condensation rate is calibrated to within 0.5 ng/cm^2 by a quartz crystal microbalance. Prior to film deposition, the Pt substrate is cleaned by resistive heating to 800 °C, and/or 500 eV Ar^+ sputtering. The evaporation temperature of $\leq$100 °C is well below the thymine decomposition temperature of about 320 °C. X-ray photoelectron spectroscopy and thin film chromatography results show that the films consist of intact molecules [16,17]. The sample film is positioned in the center of the reaction chamber at 2 cm from both the exit of the ion beam line and the entrance of the mass spectrometer,

with an incident beam angle of 30° and QMS observation angle of 60°, both with respect to the sample surface, and subjected to ion irradiation. In the ion stimulated desorption mode, positive and negative ions that desorb *during* primary ion impact at a fixed beam energy are recorded as a function of mass/charge ratio. The base pressure in the target chamber during experiments is $\sim 2 \times 10^{-9}$ Torr.

With a co-axial, low profile ionizer (open grid on line of sight) installed between the entrance ion optics and the quadrupole mass filter, the QMS is also used in the residual gas analyzer (RGA) mode to fragment and ionize neutral gas phase molecules. The results of electron impact on thymine in the gas phase, presented here, were taken in this mode with the electron impact energy set at 70 eV. The electron impact mass spectra were obtained after careful baking of the UHV system and degassing of the sample in the load-lock chamber to reduce the RGA background signal (particularly the H_2^+ and H_2O^+) to minimum. A relatively large amount of thymine is deposited on the Pt substrate, which is then placed in front of the entrance of the QMS. Subsequently, the thymine molecules are gently evaporated from the Pt into the QMS, by warming up the Pt substrate to 85–95 °C, and subjected to electron impact. For the moment, only cation yields can be recorded during *electron impact*, i.e., when the QMS is used *in the RGA neutral detection mode*; installation of a RGA anion option may soon allow neutral detection in the RGA mode via 4–20 eV dissociative electron attachment (however, in the ion stimulated desorption mode the ionizer is turned off, and both *desorbing* anions and cations are detected by the QMS). A background spectrum, taken immediately prior to the sample evaporation, is subtracted from the thymine electron impact mass spectra presented here. The gas phase electron impact mass spectra obtained here can more easily be compared directly to our ISD mass spectra, since the QMS filter and detection system are the same for both measurements; thus, we can ignore differences in transmission and detection efficiencies between our QMS and mass spectrometers used in previous measurements of electron impact on thymine [18].

To facilitate chemical identification of the fragments, thymine (T) and partially deuterated thymine (thymine-methyl-d_3-6-d) were used in all of the present experiments. The stated purities are 99% for T, and 99% isotopic purity for T_d (both from Sigma–Aldrich); to remove impurities prior to evaporation, all compounds are gently degassed in the separate load-lock chamber by heating for several hours near 40 °C, well below the evaporation onset for thymine (ca. 65–75 °C).

3. Results and discussions

3.1. Positive ion formation

Both electron and ion impact on thymine produces abundant cation fragments. Fig. 2 shows typical mass patterns of positive ion fragments produced by: (a) 70 eV electron impact in the gas phase and (b) 200 eV Ar^+ ion irradiation of a 200 ng/cm^2 thymine film on Pt. The molecular parent cations are observed at 126 and 127 amu, respectively, for electron and ion impact. The appearance of the parent ion at 127 amu during ion irradiation of the film is due to protonation. Protonation is frequently observed during surface desorption, such as secondary ion mass spectrometry, and is also observed in the production of daughter ions as discussed below.

During Ar^+ ion irradiation of thymine films, three fragment peaks are observed at 109–111 amu, which can be

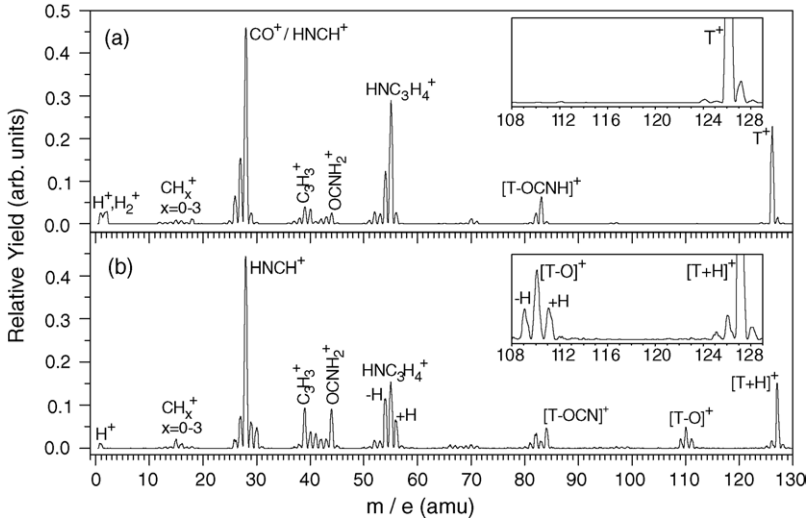

Fig. 2. Global positive ion fragmentation pattern from thymine (T) produced by: (a) 70 eV electron impact in the gas phase and (b) 200 eV Ar^+ ion irradiation of a 200 ng/cm^2 thymine film on Pt substrate. The insets shows the parent molecular ions, and a fragment from the loss of an oxygen atom induced by Ar^+ ion irradiation in (b). The chemical identification of the fragments is discussed in detail in the text. Both mass spectra have been normalized in intensity, such that the integral intensity of either mass spectrum from 0 to 200 amu is equal to 1.

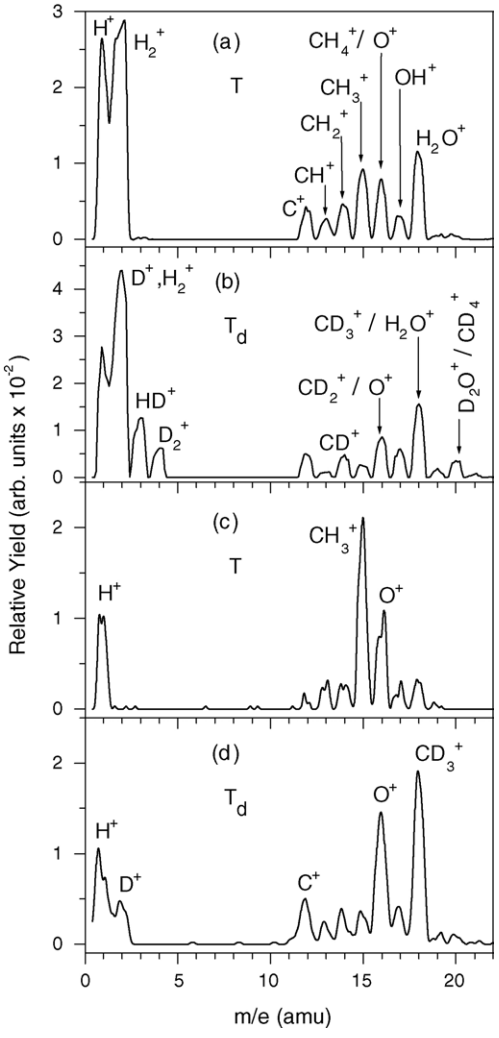

Fig. 3. Close up of cation mass spectra between 0 and 22 amu induced by 70 eV electron impact on: (a) gas phase thymine (T) and (b) gas phase thymine-methyl-d_3-6-d (T_d), and 200 eV Ar^+ impact on 200 ng/cm^2 films of: (c) thymine (T) and (d) thymine-methyl-d_3-6-d (T_d) on a Pt substrate. The relative ion intensity ($\times 10^{-2}$) is in arbitrary units (see Fig. 2).

assigned to the loss of an oxygen atom from thymine $[T–O]^+$ and its derivatives $[T–O \pm H]^+$. It is not clear whether this fragment involves breaking of endocyclic bonds. These peaks are not seen in the mass spectrum of electron impact, suggesting the absence of this specific oxygen loss fragmentation channel.

As shown in Fig. 3, in the region of 0–22 amu, we observe hydrocarbon fragments CH_x^+ ($x = 0$–3), and H^+ fragments for Ar^+ impact on films of T. These fragments are more clearly observable when we use low mass cations, such as He^+ or N^+. He^+ ion impact of thymine in particular also leads to enhanced H^+ desorption via a specific reactive scattering channel, and will be discussed elsewhere [19]. Below 22 amu, 200 eV Ar^+ impact on T films yields mainly CH_3^+ and some O^+ fragments (the 15 amu CH_3^+ peak from Ar^+ irradiation of T films shifts to 18 amu CD_3^+ in T_d films, the 16 amu O^+ peak does not shift between T and T_d; see Fig. 3c and d), as well as H^+ from both NH and CH sites. Despite the very low H^+ intensity, it seems there is a 2:1 preference for N–H compared to C–H bond cleavage, in contrast to the stoichiometric ratio of 1:2 for NH and CH sites. Seventy electron volt electron impact on gas phase T may result in H^+, H_2^+, O^+, CH_n^+ ($n = 0$–4), OH^+, and H_2O^+ elimination. As seen in Fig. 3a and b, the identification of possible CH_4^+ production is however complicated by the fact that for gas phase T_d, the 20 amu (CD_4^+) and 19 amu (CD_3H^+) peaks from electron impact may have contributions from D_2O^+ (20 amu) and HDO^+ (19 amu). Most of the H^+, H_2^+, and a significant fraction of the OH^+ and H_2O^+ are believed to result directly from gas phase electron–thymine interactions, since: (a) their yields are substantially larger than that observed in the subtracted background mass spectrum and (b) a significant yield of their deuterated analogs is observed for gas phase T_d (Fig. 3b). However, a small contribution from residual water and H_2 in the UHV chamber cannot be ruled out for the electron impact spectra below 20 amu.

In order to facilitate fragment identification, close ups of the mass spectra for the major fragments of thymine-methyl-d_3-6-d produced by electron and ion impact are shown in Figs. 4 and 5, respectively, along with those of thymine. We first discuss the assignments from high *m/e* fragments to low *m/e* fragments (from right to left of both figures).

In the gas phase electron impact spectra shown in Fig. 4, the fragment of thymine at 83 amu is found to shift to 87 amu in the case of T_d, indicating that it contains the four deuterium atoms. This fragment is assigned to the loss of an OCNH group from thymine. Further loss of a hydrogen gives a fragment at 82 amu, which shifts to 85 and 86 amu in the mass spectrum of thymine-methyl-d_3-6-d as a result of further loss of carbon-bound deuterium or nitrogen-bound hydrogen, respectively. The branching ratio between mass 85 and 86 amu in T_d is in reasonable agreement with the stoichiometric ratio of 2:1 for CD and NH sites.

In the ion impact mass spectra on T and T_d films in Fig. 5, most of the $[T–OCNH]^+$ (83 amu) or $[T_d–OCNH]^+$ (87 amu) fragments desorbs in the *protonated* form as $[T–OCN]^+$ or $[T_d–OCN]^+$ at 84 or 88 amu, respectively. Loss of hydrogens from $[T–OCNH]^+$ yields fragments at 82 and 81 amu, while loss of H or D from $[T_d–OCNH]^+$ yields fragments at 86 and 85 amu, which is in agreement with the assignment of this fragment from the gas phase electron impact mass spectra of T and T_d.

The fragment at 55 amu from electron impact (Fig. 4) is assigned to $HNC_3H_4^+$ as it shifts to 59 amu in the case of T_d. Further loss of a hydrogen (deuterium) atoms gives fragment(s) at 54 amu (for T) and 57 and 58 amu (for T_d). A possible fragment $OC_3H_3^+$ may also contribute to the peak at 55 amu, which should shift to 58 amu ($OC_3D_3^+$) in the case of T_d. However, further loss of a deuterium from this 58 amu fragment should yield a fragment at 56 amu in the case of T_d, the low yield of which suggests a negligible contribution of this dissociation channel.

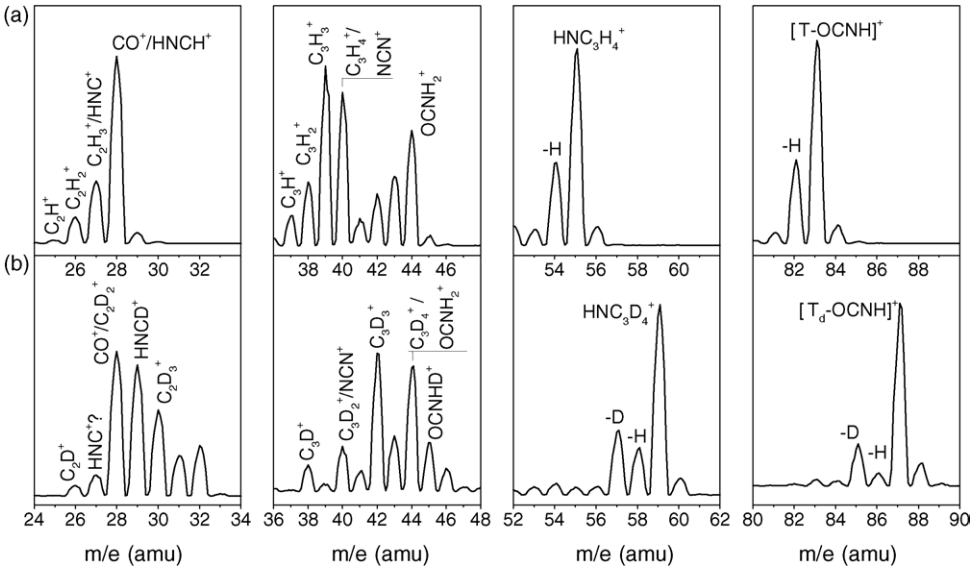

Fig. 4. Detailed positive ion fragment patterns produced by 70 eV electron impact on: (a) thymine (T) and (b) thymine-methyl-d_3-6-d (T_d), both in the gas phase. The relative ion intensity is in arbitrary units (see Fig. 2).

During Ar^+ ion irradiation of T and T_d films (Fig. 5), part of the $HNC_3H_4^+$ (55 amu) and $HNC_3D_4^+$ (59 amu) fragments appear in protonated form (56 and 60 amu). However, as seen in Fig. 5, the loss of a hydrogen from the 55 amu $HNC_3H_4^+$, resulting in desorption of a 54 amu fragment, may involve hydrogen loss from either NH or CH groups, i.e., formation of $NC_3H_4^+$ or $HNC_3H_3^+$, since for T_d films both 58 and 57 amu fragments are observed, i.e., $NC_3D_4^+$ and $HNC_3D_3^+$. In either case, $HNC_3H_4^+$ is the second most dominant cation fragment.

In the 36–48 amu region, both gas phase electron impact on T (Fig. 4) and Ar^+ ion irradiation of T films (Fig. 5) produce a series of hydrocarbon fragments $C_3H_x^+$ ($x = 1$–4) at 37–40 amu, which shift to 38, 40, 42, and 44 amu in the case of T_d. For Ar^+ impact on T films (Fig. 5), these fragments are dominated by $C_3H_3^+$. The fragment at 44 amu from T by both Ar^+ and electron impact may be assigned to $OCNH_2^+$, and may be the result of the O atom in the $OCNH^+$ fragment abstracting a neighboring hydrogen from either the $–CH_3$ group or an N–H site prior to fragmentation, or desorption. Thus, this fragment can contribute to both the 44 amu ($OCNH_2^+$) and 45 amu ($OCNHD^+$) fragments in the case of T_d, which excludes residual CO_2 as a major contribution to the 44 amu peak in the thymine mass spectra. The

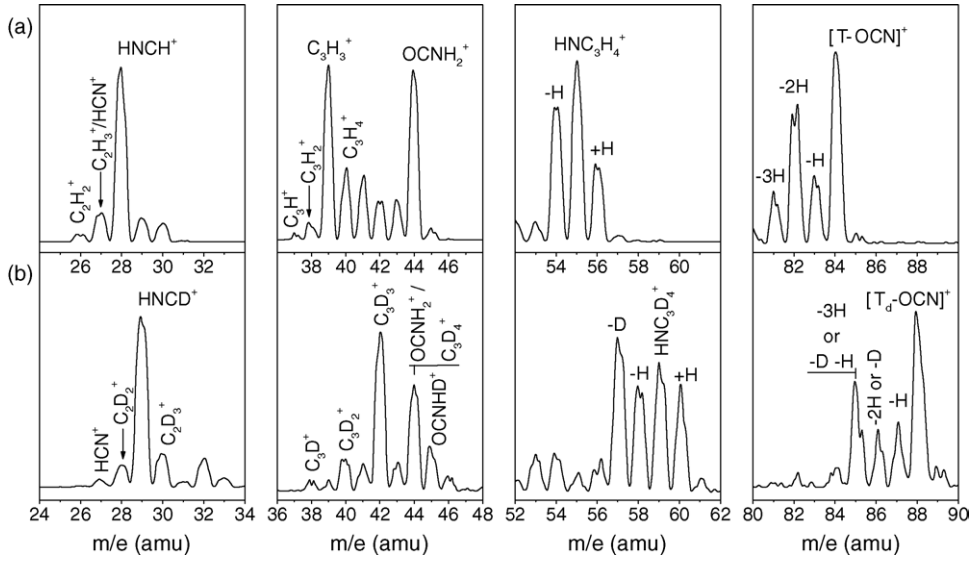

Fig. 5. Detailed positive ion fragment patterns produced by 200 eV Ar^+ ion irradiation of 200 ng/cm^2 films of: (a) thymine (T) and (b) thymine-methyl-d_3-6-d (T_d), both on a Pt substrate. The relative ion intensity is in arbitrary units (see Fig. 2).

41–43 amu fragments from T are presently unassigned, and a minor contribution of NCN^+ to the 40 amu fragment cannot be excluded.

Between 24 and 34 amu, we find the dominant cation fragments produced by both electron and ion impact. However, the gas phase electron impact spectra become complicated in the case of T_d. Instead, we first discuss the condensed phase ion impact spectra in Fig. 5.

For ion impact on T films, the dominant fragment shifts from 28 amu in T to 29 amu in T_d, indicating the inclusion of a deuterium atom in the fragment, and thus presence of a hydrogen atom in the case of T. As a consequence, this fragment is uniquely and exclusively assigned to $HNCH^+$ ($HNCD^+$) as the first dominant fragment, and not CO^+. The other minor fragments in this region are assignable to hydrocarbon fragments $C_2H_x^+$ ($x = 1$–3) and possibly a minor contribution from HCN^+ (27 amu).

During gas phase electron impact (Fig. 4), the spectrum of T is similar to that of ion impact, but that of T_d is quite different. First of all, we can assign the hydrocarbon fragments $C_2D_x^+$ ($x = 1$–3) at 26, 28 and 30 amu, and fragment $HNCD^+$ at 29 amu. Judging from the branching ratios of $C_2H_x^+$ and $C_2D_x^+$ fragments, the 28 amu peak has another major contribution from CO^+, which is absent in the case of ion irradiation. For gas phase electron impact on T, a possible contribution from background N_2 and/or CO to this 28 amu peak is excluded because: (1) a background spectrum has been subtracted from the spectra in Fig. 4 and (2) the 28 amu peak of the background spectrum exhibits no significant increase when warming up a clean Pt substrate following the same procedure used to take the electron impact spectra of gas phase thymine and thymine-methyl-d_3-6-d. Hence, in the gas phase electron impact spectrum of thymine (Fig. 4), the 28 amu peak contains contributions from both $HNCH^+$ and CO^+, while in the condensed phase ion impact spectrum (Fig. 5), it consists uniquely of the $HNCH^+$ fragment. This suggests the absence of a specific CO^+ fragmentation channel in the case of ion impact on thymine films.

Notably, during ion impact on T_d and T films, we also find that hydrogen (or proton) pickup by certain fragments prior to desorption involves predominantly abstraction of a hydrogen (or proton) from the NH sites in adjacent T_d (or T), and not the CD (or CH) sites (e.g., for T_d films in Fig. 5, we observe mainly $[HNC_3D_4 + H]^+$, not $[HNC_3D_4 + D]^+$). Conversely, hydrogen loss from a specific fragment during its collisions in the film prior to desorption may involve both the fragment's NH and CD (or CH) sites (e.g., a $[HNC_3D_4]^+$ fragment from T_d may scatter in the film prior to desorption and lose either a D or H, resulting in desorption of both $[NC_3D_4]^+$ and $[HNC_3D_3]^+$ fragments; Fig. 5). The former point is also observed in the desorption of the protonated parent molecule from films of T and T_d as shown in Fig. 6. From integration of the mass peak signals, we find that for $[T + H]^+$ formation and desorption, there appears a strong 4:1 preference for abstraction of nitrogen-bound hydrogens, relative to carbon-bound hydrogens, opposed to the stoichiometric ratio of NH to CH

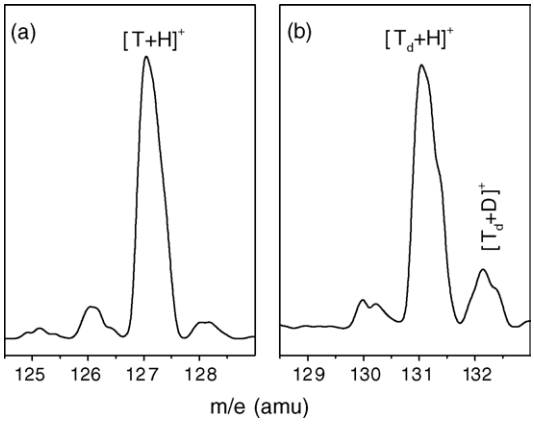

Fig. 6. Detailed view of ion stimulated desorption (ISD) mass spectra for parent molecule $[M + H]^+$ formation by 200 eV Ar^+ impact on 200 ng/cm^2 films of: (a) thymine (T) and (b) thymine-methyl-d_3-6-d (T_d), both on a Pt substrate. The relative ion intensity is in arbitrary units (see Fig. 2).

sites of 1:2. This strong preference for formation of $[T_d + H]^+$ versus $[T_d + D]^+$, even when accounting for small quantities of natural ^{13}C in T or T_d, e.g., $[T_d(^{13}C) + H]^+$ (132 amu), may be the result of the relatively weaker binding energy of NH compared to CH bonds in thymine. Such protonation is not observed in gas phase electron impact, due to the absence of adjacent molecules; however, during gas phase electron impact ionization, some bond rearrangement and nuclear motion (atom scrambling) may occur during the lifetime of the dissociating parent cation, and lead to elimination of H_2^+, OH^+, H_2O^+, or $OCNH_2^+$. In large gas phase polyatomic molecules, this is attributed to the lack of competing decay channels of the parent cation state during dissociation, which has sufficient time to evolve along the potential energy landscape towards various dissociation asymptotes, some of which yield to molecular rearrangement during dissociation [20].

3.2. Negative ion formation

Fig. 7 shows the negative ion ISD mass pattern produced by 200 eV Ar^+ ion irradiation of a 20 ng/cm^2 thymine film on Pt substrate. Most of the anion fragments are more clearly observable at low coverage, which is related to their specific fragmentation dynamics [15]. The major fragments at 1, 16, 26, 42, and 125 amu are assigned to H^-, O^-, CN^-, OCN^-, and $[T–H]^-$. With the exception of H, the known electron affinities (EA) [21] of these intense fragments are quite high, i.e., 1.46 eV (O), 3.86 eV (CN), and 3.6 eV (OCN), compared to 0.75 eV for H; here, the $[T–H]^-$ fragment involves deprotonation almost exclusively at the NH sites (to be discussed below), and its EA has been estimated to be between 3 and 4 eV [22]. In any case, the strong intensity of these fragments suggests that their EA's contribute to their formation mechanism by low energy ion impact [15].

The minor anion fragments in Fig. 7 are assigned to CH^-, OH^-, C_2^-, C_2H^-, C_2CN^-, C_2OCN^-, $NC_3H_2^-$, $HNC_3H_3^-$,

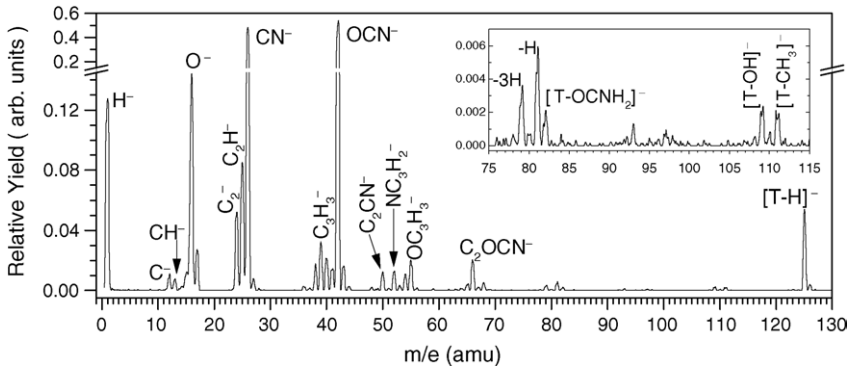

Fig. 7. Global negative ion fragment ISD pattern of thymine (T) produced by 200 eV Ar^+ ISD of a 20 ng/cm^2 thymine film on Pt substrate. The inset shows an enlargement of the region from 75 to 115 amu. The spectrum has been normalized in intensity, such that the integral intensity from 0 to 200 amu is equal to 1. The chemical identification of the fragments is discussed in detail in the text.

$OC_3H_3^-$, and hydrocarbon fragments $C_xH_y^-$. While the fragments such as $NC_3H_2^-$, $HNC_3H_3^-$, and $OC_3H_3^-$ originate from direct fragmentation of thymine, there may be a contribution from carbon impurities in the Pt substrate to C^-. The small yield of mass 109 and 111 amu fragments in Fig. 7 is tentatively assigned to $[T–OH]^-$ and $[T–CH_3]^-$, respectively. While the latter assignment is consistent with a shift from 111 to 112 amu ($[T_d–CD_3]^-$) upon T_d substitution (not shown), this is complicated by the fact that the 109 amu peak also shifts to 112 amu, suggesting $[T_d–OD]^-$ formation. The slightly larger peaks at 79, 81, and 82 amu are not yet assigned, but may in principle result from $[T–OCNH_2–nH]^-$ ($n = 0$, 1, and 3) formation; however, the presence of trace amounts of 5-bromouracil contaminants in the sample might also yield 79 and 81 amu anions ($^{79,81}Br^-$).

Analogous to the cation fragments, Fig. 8 allows identification of many of the anion species produced by Ar^+ impact by comparing results from T and T_d films from high to low mass fragments. For T films, the 66 amu fragment is assigned to C_2OCN^-, which does not shift when T_d is substituted for T. The small 68 amu satellite peak from T is tentatively assigned to $[C_2OCN + 2H]^-$ since it shifts to 69 amu, viz. $[C_2OCN + H + D]^-$. However, it may also be related to the 64/65 amu peaks from T which remains unassigned. Between 48 and 60 amu for T, we find a unique fragment pattern with peaks at 50, 52, 54, and 55 amu, the first of which

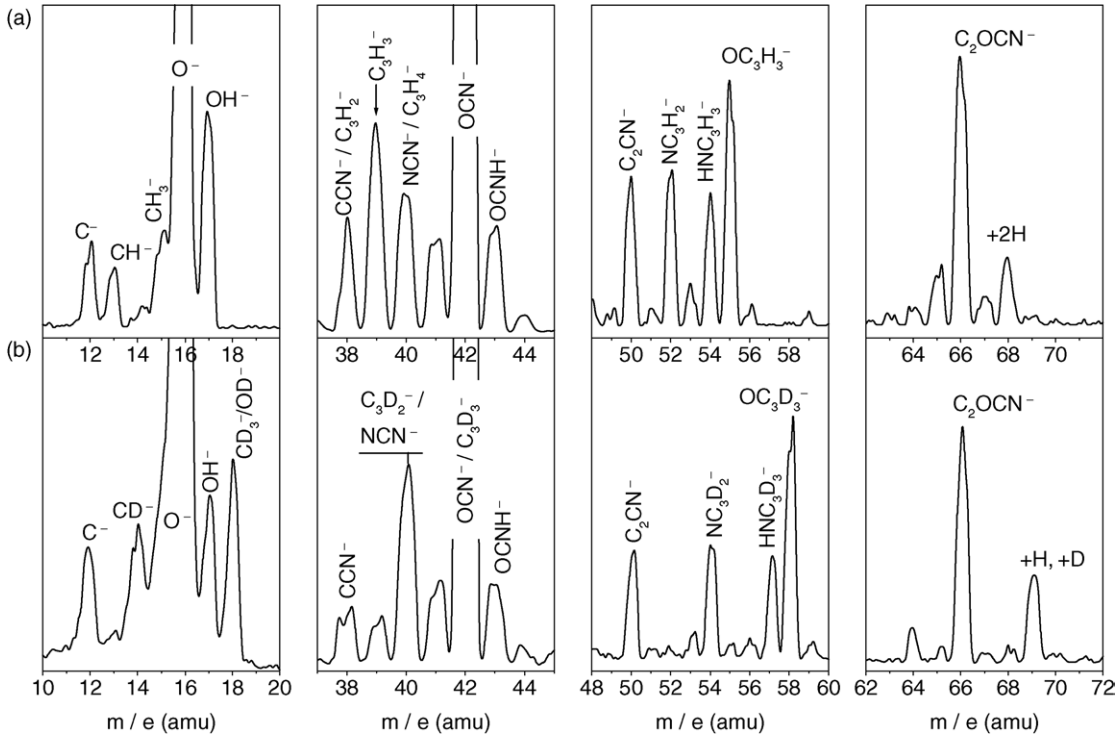

Fig. 8. Detailed negative ion fragment patterns produced by 200 eV Ar^+ ion irradiation of 20 ng/cm^2 films of: (a) thymine (T) and (b) thymine-methyl-d_3-6-d (T_d), both on a Pt substrate. The relative ion intensity is in arbitrary units (see Fig. 7).

is assigned here to C_2CN^-, since it does not shift upon T_d substitution. The latter three are assigned to $NC_3H_2^-$, $HNC_3H_3^-$, and $OC_3H_3^-$; for T_d substitution, this three peak pattern shifts to 54 amu ($NC_3D_2^-$), 57 amu ($HNC_3D_3^-$), and 58 amu ($OC_3D_3^-$), whereby the lack of a 59 amu peak ($HNC_3D_4^-$) precludes contributions of a $HNC_3H_4^-$ fragment to the 55 amu peak from T.

Except for OCN^-, the sequence of fragments between 37 and 45 amu in Fig. 8 is more difficult to interpret, since more than one fragment may in principle contribute to the peaks at 38 and 40 amu in T films. Hence, some of the anion peaks in the 37–45 amu range in Fig. 8 are only tentatively assigned. However, we note that: (a) the 37 amu peak in T is most likely $C_3H_3^-$, since C_3H_3 has an EA of 2.7 eV, and it is almost completely absent in T_d, where a $C_3D_3^-$ fragment would contribute to the already very intense OCN^- peak at 42 amu, and (b) the 43 amu peak in T does not shift in T_d, suggesting formation of $OCNH^-$ involving either of its two NH positions in T; this seems reasonable since it involves cleavage of two bonds, rather than three if the hydrogen in $OCNH^-$ were to originate from H abstraction at a carbon site. Moreover, since the peak at 40 amu in T does not shift to 44 amu in T_d, it is likely that it originates from the formation of CN_2^- (EA of CN_2 is 1.8 eV) and not $C_3H_4^-$.

The peak assignments at 24 and 25 amu in T films to C_2^- and C_2H^- in Fig. 7 are confirmed by the observation that for T_d films, the 24 amu peak is unchanged while the 25 amu peak is absent (not shown), since the C_2D^- fragment (26 amu) will contribute to the strong CN^- peak. We note that both the C_2 and C_2H have high EA's of 3.3 and 3 eV [21], respectively, which may contribute to their formation mechanism. Between 10 and 20 amu for T (Fig. 8), we find that the CH^- peak at 13 amu in T shifts to 14 amu in T_d, and thus suggests assignment to CD^-. The 17 amu peak in T is assigned to OH^-, since it shifts to 18 amu in T_d; since this is also associated with a shift of CH_3^- (15 amu) to CD_3^- (18 amu), this assignment is more tentative. However, we find that upon T_d substitution, the OH^- peak decreases in relative intensity, while the 18 amu peak increases more than can be accounted for by the small amount attributable to CD_3^-. Thus, the 18 amu peak is mainly attributed to OD^-. Since the thymine molecules here have no OH groups, this suggests that here some of the large amount of O^- formed by ion impact in the film may react by H abstraction prior to desorption as OH^- or OD^-. This mechanism has been observed in electron irradiated mixed films of O_2 containing hydrocarbons [23]. Here, the observation that both OH^- and OD^- can be formed in T_d films, suggests that H abstraction by desorbing O^- occurs at both CH and NH sites.

Regarding the formation of the lowest and highest mass anions, i.e., H^- and $[T–H]^-$, we note that the site of H removal is not identical to both. This is shown in Fig. 9, which shows that while H^- and D^- formation from T_d occurs with 1:2 stoichiometric ratio, deprotonation of T (or T_d) seems to clearly occur mainly at the NH sites, and almost always results in formation of $[T–H]^-$ (125 amu) and $[T_d–H]^-$ (129 amu). This suggests that the formation mechanisms are likely different for $H^-(D^-)$ than for $[M–H]^-$ formation [15].

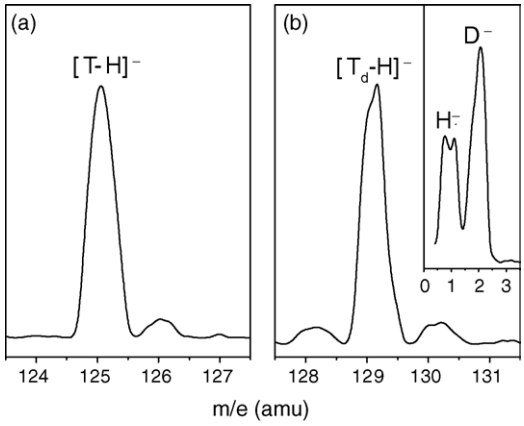

Fig. 9. Detailed view of ion stimulated desorption (ISD) mass spectra for parent molecule $[M–H]^-$ formation by 200 eV Ar^+ impact on 20 ng/cm^2 films of: (a) thymine (T) and (b) thymine-methyl-d_3-6-d (T_d), both on a Pt substrate. The inset in (b) shows the H^- and D^- yield from T_d. The relative ion intensities are in arbitrary units (see Fig. 7).

3.3. Fragment origins and desorption energy thresholds

Given the chemical identification of several ionic fragments, it is possible to further specify their site origins within the thymine molecule. According to the molecular structure of thymine, the major cation fragment $HNCH^+$ ($HNCD^+$) is a result of cleaving the N(1)–C(2) bond and the C(5)–C(6) bond, and the $HNC_3H_4^+$ ($HNC_3D_4^+$) fragment is a result of breaking the N(1)–C(2) bond and the C(4)–C(5) bond. Fragment $C_3H_3^+$ ($C3D3^+$) arises from dissociation of the N(1)–C(6) bond and the C(4)–C(5) bond, with further loss of a hydrogen atom. The fragments $[T–OCNH]^+$, $OCNH_2^+$, CN^-, and OCN^- can have three possible site origins, which are not distinguishable on the basis of the present results. Fragments $[T–O]^-$, O^-, $H–/H^+$, and CH_3^+ are results of breaking specific exocyclic bonds of thymine.

Since the fragmentations involve either endocyclic or exocyclic bond cleavage, both the positive and negative ion fragments can be sorted into two groups. In this respect, the cation fragments $HNCH^+$, $C_3H_3^+$, $OCNH_2^+$, $HNC_3H_4^+(\pm H)$, and $[T–OCNH]^+(\pm H)$, and the anion fragments CN^- and OCN^- clearly indicate endocyclic bond cleavage, while the H^+, CH_3^+, $[T–O]^+(\pm H)$, H^-, and O^- originate from exocyclic bond cleavage. Thus, one is able to identify ion impact damage to the endocyclic and the exocyclic sites in thymine, as well as the dependence of fragment desorption on incident ion projectile and energy.

Fig. 10 shows the relative yields of cation fragment desorption as a function of incident energy during Ar^+ ion irradiation of a 200 ng/cm^2 thymine film, from which the desorption energy thresholds of major fragments can be approximated. Most cation fragments appear at energies near 15–30 eV, namely $HNC_3H_4^+$ (15–18 eV), $HNCH^+$, $[T–OCNH]^+(\pm H)$,

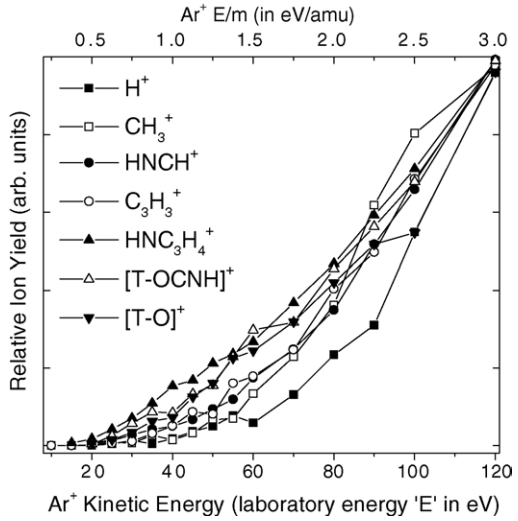

Fig. 10. Relative yields of positive ion fragment desorption as functions of incident ion energy during Ar^+ ion irradiation of a 200 ng/cm^2 thymine film on Pt substrate. The yield curves for the various ions have been normalized here in intensity at 120 eV to compare their energy dependence. Their relative abundance can be seen in Fig. 2.

$[T–O]^+(\pm H)$ (∼20 eV), and $C_3H_3^+$ (∼30 eV). The CH_3^+ and H^+ fragments appear at higher energies of about 40 and 60 eV, respectively. The anion fragments appear generally at higher energies with H^- at 40 eV, CN^- and OCN^- at 60 eV, and O^- at about 70 eV (not shown here). It is interesting to note that for Ar^+ impact, the endocyclic cation fragments $HNC_3H_4^+$, $HNCH^+$, $[T–OCNH]^+$, etc., appear at lower energies than the exocyclic fragments CH_3^+ and H^+. The detailed fragmentation dynamics leading to the observed ion desorption is discussed elsewhere [15].

Most of the major ion fragments observed here during Ar^+ ion irradiation of thymine films are also seen when we irradiate such films with other ions, including Ar^{2+}, He^+, CO^+, NO^+, O^+, N_2^+, N^+, and D_x^+ ($x = 1$–3) [19]. While the results from these latter measurements cannot be discussed here for sake of brevity, we find it worthwhile to note the general trends: (1) anion fragments appear usually at higher incident ion energies than the cation fragments. (2) High mass incident ions tend to fragment thymine molecules more efficiently than low mass ions, and also result in the desorption of larger fragment ions. For example, during 50–200 eV Ar^+ irradiation, the cation fragment spectra are dominated by $HNCH^+$, $HNC_3H_4^+$, etc., while during 50–200 eV He^+ irradiation, the H^+ fragment, instead of $HNCH^+$, dominates the cation fragment yields, which suggests an enhancement of CH or CD bond cleavage by lower mass ion projectiles. (3) The energetic sequence of damage to endocyclic and exocyclic bonds of thymine also depends on the ion projectiles. During heavy ion (Ar^+, Ar^{2+}, N_2^+, and N) impact, endocyclic fragments appear at lower energy than exocyclic fragments, while during light ion (He^+ and D_x^+ ($x = 1$–3)) impact, exocyclic fragments appear at lower energies than endocyclic fragments. These studies continue and will be discussed in detail elsewhere [19].

4. Summary and conclusions

Thymine and thymine-methyl-d_3-6-d are irradiated by low energy (10–200 eV) ions in the condensed phase, and by 70 eV electrons in the gas phase. The ionic fragmentation products are measured by a quadrupole mass spectrometer. Both electron and ion impact produces abundant positive ion fragments. The chemical composition of the ionic fragments has been identified by comparing the mass spectra of thymine and thymine-methyl-d_3-6-d. The major cation fragments produced by Ar^+ impact on thymine films are identified as $HNCH^+$, $HN(CH)CCH_3^+$, $C_3H_3^+$, $OCNH_2^+$, $[T–OCN]^+$, $[T–O]^+$, and $[T+H]^+$. While ion impact produces an additional fragment $[T–O]^+$, gas phase electron impact also leads to a fragment CO^+ that is not seen in condensed phase ion impact. The anion fragments produced by Ar^+ impact on thymine films are dominated by H^-, O^-, CN^-, and OCN^-, with smaller amounts of $NC_3H_2^-$, $HNC_3H_3^-$, $OC_3H_3^-$, and other hydrocarbon anions. Both positive and negative ion fragment desorption involves exocyclic and endocyclic bond cleavage, which extends down to about 15–18 eV for positive ion fragments.

In the radiobiological context of heavy primary ion interactions in biological media, our measurements suggest that: (a) even at primary ion track-ends, i.e., well beyond the Bragg peak, significant ion damage to cellular DNA may occur, and (b) secondary hyperthermal ions, produced anywhere along the primary ion track, are also likely to cause similar damage. In both cases, DNA damage even at the lowest ion energies, e.g., below 1 eV/amu, may involve complex fragmentation channels (damage clusters) that reach far beyond simple molecular ionization.

Acknowledgements

This work is continuously supported by the Natural Science and Engineering Research Council of Canada. A previous grant from the Canadian Institute of Health Research provided funds for the construction of the ion beam apparatus, and is hereby also acknowledged.

References

[1] C. von Sonntag, The Chemical Basis for Radiation Biology, Taylor and Francis, London, 1987.
[2] ICRU Report 31, International Commission on Radiation Units and Measurement, Washington, DC, 1979;
ICRU Report 55, 1995.
[3] V. Cobut, Y. Frongillo, J.P. Patau, T. Goulet, M.-J. Fraser, J.-P. Jay-Gerin, Radiat. Phys. Chem. 51 (1998) 229.
[4] M.D. Sevilla, D. Becker, M. Yan, S.R. Summerfield, J. Phys. Chem. 95 (1991) 3409;

P.M. Cullis, J.D. McClymont, M.E. Malone, A.N. Mather, I.D. Podmore, M.C. Sweeney, M.C.R. Symons, J. Chem. Soc., Perkin Trans. 22 (1992) 1695.
[5] B. Boudaiffa, P. Cloutier, D. Hunting, M.A. Huels, L. Sanche, Science 287 (2000) 1658.
[6] L. Sanche, Mass Spectrom. Rev. 21 (2002) 349, and references therein.
[7] M.A. Huels, I. Hahndoff, E. Illenberger, L. Sanche, J. Chem. Phys. 108 (1998) 1309.
[8] M.-A. Herve du Penhoat, M.A. Huels, P. Cloutier, J.-P. Jay-Gerin, L. Sanche, J. Chem. Phys. 114 (2001) 5755.
[9] D. Antic, L. Parenteu, L. Sanche, J. Phys. Chem. 103 (1999) 6611.
[10] D. Antic, L. Parenteu, L. Sanche, J. Phys. Chem. 104 (2000) 4711.
[11] H. Abdoul-Carime, M.A. Huels, E. Illenberger, L. Sanche, J. Am. Chem. Soc. 123 (2001) 5354.
[12] H. Stelzer, Nucl. Phys. B (Proc. Suppl.) 61B (1998) 650.
[13] M. Scholz, Nucl. Instrum. Methods Phys. Res. B 161–163 (2002) 76.
[14] T. Schlathölter, R. Hoekstra, R. Morgenstern, Int. J. Mass Spectrom. 233 (2004) 173.
[15] Z.-W. Deng, M. Imhoff, M.A. Huels, J. Phys. Chem., J. Chem. Phys., in press.
[16] D. Klyachko, T. Gantchev, M.A. Huels, L. Sanche, in: D.T. Goodhead, P. O'Neill, H.G. Menzel (Eds.), Microdosimetry: An Interdisciplinary Approach, The Royal Society of Chemistry, Cambridge, UK, 1997, p. 85.
[17] D.V. Klyachko, M.A. Huels, L. Sanche, Radiat. Res. 151 (1999) 177.
[18] NIST Database for Gas Phase Electron Impact Fragmentation of Thymine at http://webbook.nist.gov/chemistry/.
[19] M. Imhoff, Z.-W. Deng, M.A. Huels, in press.
[20] This is different to anion fragment formation via dissociative electron attachment in the gas phase, where the initial parent *anion* can also decay by electron autodetachment; for parent *cations* this decay channel is absent, while for large *polyatomic parent anions* the electron autodetachment decay channel can be significantly reduced. For a detailed discussion, see: M. Stepanovic, Y. Pariat, M. Allan, J. Chem. Phys. 110 (1999) 11376.
[21] Except where indicated, all EA's are from: J.C. Rienstra-Kiracofe, G.S. Tschumper, H.F. Schaefer III, S. Nandi, G.B. Ellison, Chem. Rev. 102 (2002) 231.
[22] G. Hanel, B. Gstir, S. Denifl, P. Scheier, M. Probst, B. Farizon, M. Farizon, E. Illenberger, T.D. Märk, Phys. Rev. Lett. 90 (2003) 188104.
[23] M.A. Huels, L. Parenteau, L. Sanche, J. Phys. Chem. B 108 (2004) 16303.